RSC Advances

COMMUNICATION

View Article Online
View Journal | View Issue

Cite this: *RSC Adv.*, 2016, **6**, 84500

Received 3rd May 2016
Accepted 30th August 2016

DOI: 10.1039/c6ra11428h

www.rsc.org/advances

Electrically active nanoantenna array enabled by varying the molecular orientation of an interfaced liquid crystal

Yu-Cheng Hsiao,[a] Chen-Wei Su,[b] Zong-Han Yang,[b] Yevheniia I. Cheypesh,[c] Jhen-Hong Yang,[b] Victor Yu. Reshetnyak,[c] Kuo-Ping Chen*[a] and Wei Lee*[a]

A system comprising a gold nanoantenna array covered with a high-birefringence liquid crystal (LC) material is introduced. By applying voltage across the LC bulk, we demonstrate that the refractive-index and polarization changes significantly modify the hybrid plasmonic–photonic resonances in the system. The hybrid structure enables the active control of the spectrum as well as a large shift in resonance wavelength of the metallic nanoantennas by means of an externally applied electric field. Our modeling supports the observed results, by assuming that the nanoantenna array leads to two orthogonal easy axes with a finite anchoring energy. In combination of the nano-structured surface with birefringent LC, tunability up to 90 nm is achieved in the visible wavelengths, opening the door towards nanoscale displays or nano-optical switches.

1. Introduction

The oscillation of free electrons in metallic nanostructures causing large electric fields near the metallic particle's surface is known as localized surface plasmon resonance (LSPR). The LSPR transforms free-space radiation into localized energy. As such, the term—optical antenna or nanoantenna—has appeared to describe metallic nanostructures with LSPRs coupled to receivers or light sources.[1] Nanoantennas possess many intriguing properties such as the directivity gain,[2–5] polarization control,[6,7] intensity enhancements,[8–10] and spectral shaping.[11] They are formed by pairs of metal nanostructures. The resonance wavelength and intensity of the localized fields in nanoantennas are strongly dependent of the structural geometry and the refractive index of the surrounding medium. It is practically significant to enable active control of these optically coupling properties by means of an external tuning technology. Such tunability can be accomplished by incorporating other materials submitted to, say, an applied voltage, heat, or illumination profile.[12–14] Recently, graphene has been integrated into nanogaps of coupled plasmonic antennas for electrical tuning of antenna resonance in the mid-infrared region.[15] However, the electrical tuning of antenna resonances in the visible is highly desired. Liquid crystals (LCs) are interesting materials in that their electrically induced re-orientation of molecules can modify the resonance conditions of optical resonators. Indeed, LCs can be employed to control resonances in metallic nanostructures, including LSPR-based nanoantennas and surface plasmon polaritons in metallic films.[16–19] To the best of our knowledge, a hybrid LC/nanoantenna structure has not been proposed until now, not to mention the investigation of the corresponding tuning properties. Besides, the tuning ranges of typical or conventional LC-based metallic nanostructures are quite limited, merely several nanometers.[20,21]

In this study we demonstrate an active LC tuning of electromagnetic (EM) resonances in periodic arrays of metallic nanoantennas. The structure consists of pairs of square gold nanobulges covered with a high-birefringence LC material. Such nanoantennas own two resonance modes that are useful for realizing extraordinarily broad shift in wavelength. The active tuning is achieved by applying voltage on the LC-plasmonic coupled system confined by the nanostructured substrate and a conducting glass substrate coated with a rubbed film of polyimide (PI) for planar alignment of the LC. Evidenced by the voltage-dependent transmission spectrum, the shift in optical resonance of 90 nm is accomplished. Based on the assumption that the nanoantenna array produces two orthogonal easy axes with finite anchoring energies, our simulation is in good agreement with the observed results.

2. Fabrication of liquid crystal-nanoantenna coupled devices

Fig. 1 shows two scanning electron microscopic images of two-dimensional gold nanostructures fabricated on an indium-tin-

[a]*Institute of Imaging and Biomedical Photonics, College of Photonics, National Chiao Tung University, Guiren Dist., Tainan 71150, Taiwan. E-mail: kpchen@nctu.edu.tw; wlee@nctu.edu.tw*

[b]*Institute of Photonic System, College of Photonics, National Chiao Tung University, Guiren Dist., Tainan 71150, Taiwan*

[c]*Physics Department, Taras Shevchenko National University of Kyiv, Kyiv, 01601, Ukraine*

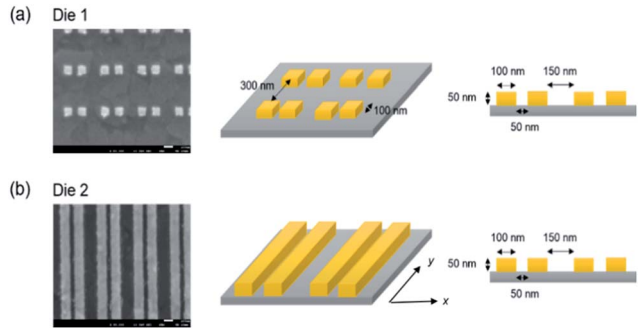

Fig. 1 Scanning electron micrographs of gold nanoantenna arrays in (a) die 1 and (b) die 2.

oxide (ITO)-coated glass substrate by well-controlled e-beam lithography. Each square gold nanoparticle in the array in die 1 (Fig. 1(a)) has x–y dimensions of 100 nm by 100 nm. The thickness (or height) of the nanoantenna array is 50 nm, and the gap between two paired square nanoparticles is also 50 nm. The periodicity of the nanoantenna dimers is 400 nm in both the x- and y-directions. Comparatively, the paired strip nanoantennas in die 2 (Fig. 1(b)) have the same dimension in the x-direction and the y dimension is 100 μm, which allows die 2 to be regarded as a grating. The substrate with the nanostructured surface serves as the bottom substrate for the LC cell as shown in Fig. 2. The other substrate is a typical ITO-coated glass slide spin-coated with a PI alignment layer and treated with mechanical buffing along the x-direction. The assembled cell has a thickness (*i.e.*, cell gap) of *ca.* 10 μm, as determined by silica spacers. A high-birefringence LC material[22] with a wide nematic range from −30.0 to 95.0 °C was introduced into the empty cell. The optical properties of the LC at 589 nm and 20 °C are: birefringence $\Delta n = 0.333$; refractive indices $n_e = 1.851$ and $n_o = 1.518$. The top and bottom electrodes permit AC voltage to be applied across the cell thickness. Linearly polarized white light transmits through the top glass substrate and the LC layer successively, and then couples to the nanoantennas with plasmonic resonance. The LSPR can be adjusted by the dielectric constant of the surrounding material; *i.e.*, the LC, which is, in turn, determined by the reorientation of the nematic director induced by the externally applied electric field at 1 kHz. The square dimers of nanoantennas combined with LC susceptible to stimuli such as an electric field provide the tunability in resonance wavelength (and color), whereas the paired strips of nanoantennas are utilized to demonstrate the switchability in intensity as a binary grey-level controller.

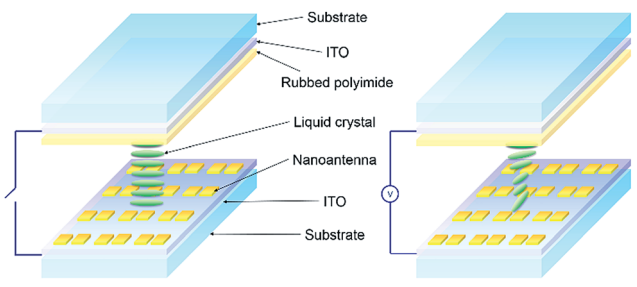

Fig. 2 Schematic of the LC cell with a nanoantenna-patterned surface on the bottom substrate. An applied electric field across the cell reorients the nematic molecules and, in turn, changes the wavelength of resonance.

3. Results and discussion

Fig. 3 compares the far-field transmission spectra acquired with finite element method (FEM) simulations for die-1 nanoantenna array at wavelengths from 600 to 900 nm. In the simulation the loss factor of the gold Drude model is 3.[23] The refractive index of the substrate is 1.52, and the ITO layer is not included in the simulation model. As the surrounding medium is anisotropic LC with high birefringence, normal-incidence spectra illuminated by linearly polarized EM waves with both x- and y-polarizations were simulated and the results are shown in Fig. 3. One can see that, in the x-polarization condition, the resonance wavelength is 780 nm and there is strong localized electric-field enhancement in the small gap correspondingly. When the polarization changes to the y-direction, the LSPR wavelength shifts to 680 nm.

Fig. 4 and 5 illustrate the observed transmittance of the LC cell at various applied AC voltages in the x- and y-polarization conditions. The experimentally measured transmittance for a specific nanoantenna pattern, either die 1 (Fig. 4) or die 2 (Fig. 5), is dependent of both the wavelength and the polarization direction of the incident light, and the spectrum varies with the applied voltage which determines the orientation of the optic axis of the uniaxially anisotropic LC. A much greater voltage is required to reorient the LC molecules near the nanostructure due to the significant strength of the anchoring force by the gold nanostructure. Fig. 4 shows that the polarization remains unchanged and the primary resonance occurs at the wavelength of 780 nm when the x-polarized incident light goes through the planar-aligned LC layer at 0 V_{rms} (left panel in

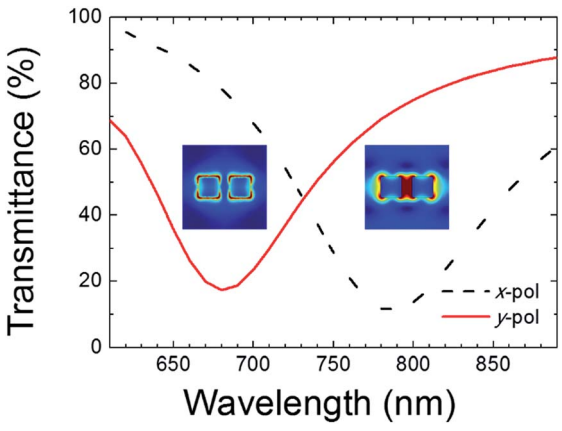

Fig. 3 Simulated far-field spectra of the die-1 nanoantenna array for linearly polarized EM waves with the x- and y-polarizations. The resonance wavelength shifts from 780 to 680 nm when the polarization changes from the x- to the y-polarization. The insets depict the localized EM field distributions.

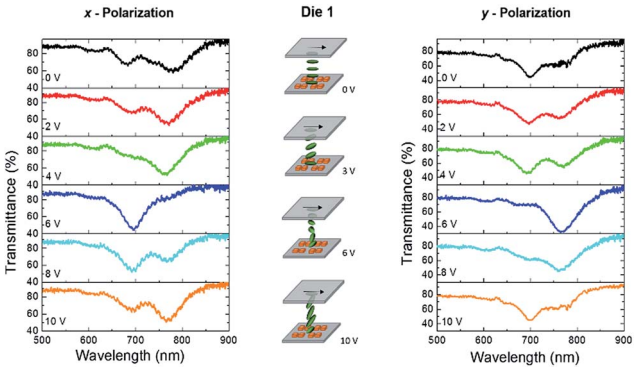

Fig. 4 Transmission spectra of the LC cell with the die-1 nanoantenna array on the bottom substrate at various applied voltages under the *x*- and *y*-polarizations.

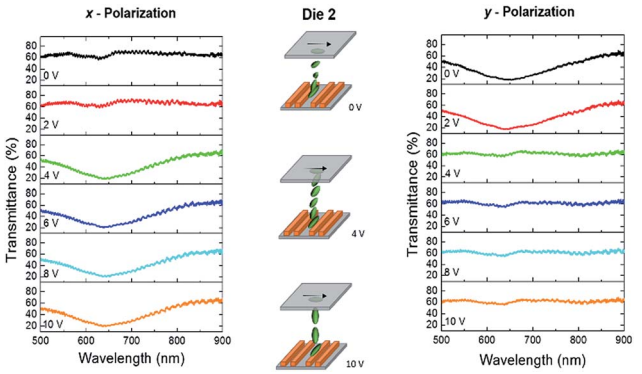

Fig. 5 Transmission spectra of the LC cell with the die-2 nanoantenna array on the bottom substrate at various applied voltages under the *x*- and *y*-polarization conditions.

Fig. 4). This unperturbed condition favours the alignment of the LC in the neighbourhood of the bottom substrate to be in parallel to the *x*-direction. The nanostructured surface does not render a strong unidirectional aligning effect on the anchoring of LC molecules near the bottom substrate. As a result, some ill-aligned LCs along the *y*-direction can bring about the noise resonances at 0 V_{rms}. At applied voltages 1–4 V_{rms} the LC molecules in the mid-plane tilt, causing the slight blueshift of the 780 nm resonance as a response to the reduced effective index refraction ($n_{eff} < n_e$). When the applied voltage increases to 5 V_{rms}, the LC starts to take the twisted nematic configuration to impose the incident *x*-polarized light to change its polarization when the light finally emerges from the bottom substrate. The resonance wavelength blueshifts to 690 nm, virtually following the 90°-twist waveguide effect of LC. Noticeably, the primary resonance at a voltage beyond 9 V_{rms} reverts to the initial wavelength of 780 nm (as is at null voltage) for the incident *x*-polarized light in that the LC becomes unwound at such a high voltage. This can be understood because the optic axis along the vertical direction in the resulting homeotropic configuration does not alter the polarization state. Moreover, the spectral features for the *y*-polarized light impinging onto the cell at increasing voltages can be explained by the same reason; namely, the change in LC configuration from the planar state at 0 V_{rms}, to the 90°-twisted state to permit the adiabatic following of the incident light at mid-voltages, and finally to the homeotropic state at, say, 10 V_{rms} (right panel in Fig. 4). The observed wavelength shift of 90 nm is reasonably close to the predicted 100 nm shift for the bare nanostructured substrate (see Fig. 3). The 10% deviation is presumably due to fabrication tolerances. Here the change in plasmonic resonance wavelength enables optical switching in nanophotonic devices.

The numerical modelling of the transition from the planar state to the twisted nematic configuration under an external electric field is essential to examine the observed phenomenon. Because our nanostructures is two dimension, the two easy axis model is used legitimately. Let us consider an initially planar-aligned nematic LC cell with strong anchoring and the easy axis direction given by $e_t = (1, 0, 0)$ at the top substrate ($z = L$). Assume that the LC on the bottom substrate (at $z = 0$) has two mutually orthogonal easy axes described by $e_b = (\cos \varphi_0, \sin \varphi_0, 0)$, where one is at $\varphi_0 = 0$ with the azimuthal anchoring energy coefficient W_2, and the other easy axis corresponds to $\varphi_0 = \pi/2$ with the anchoring energy coefficient W_1. Following the work of Fukuda *et al.*[24] the energy density can be written as the form with functional dependence of the director anchoring in the azimuthal plane:

$$F_s = -\frac{1}{2}W_1 \sin^4 \varphi(0) - \frac{1}{2}W_2 \cos^4 \varphi(0) \quad (1)$$

At the bottom substrate the anchoring is assumed to be strong for the polar director angle $\theta(0) = 0$. We shall describe the LC director distortion in terms of the angles θ and φ given by

$$n = (\cos \theta \cos \varphi, \cos \theta \sin \varphi, \sin \theta) \quad (2)$$

The strong director anchoring in the polar plane results in the following boundary conditions for the angle θ

$$\theta(0) = \theta(L) = 0 \quad (3)$$

The free energy per unit surface area of the LC layer is given by

$$F = \frac{1}{2}\int_0^L \Big[(K_{11}\cos^2\theta + K_{33}\sin^2\theta)(\theta')^2 + (K_{22}\cos^2\theta + K_{33}\sin^2\theta)\cos^2\theta(\varphi')^2 - \varepsilon_0\varepsilon_a E^2 \sin^2\theta\Big]dz - \frac{1}{2}W_1 \sin^4\varphi(0) - \frac{1}{2}W_2\cos^4\varphi(0) \quad (4)$$

The corresponding Euler–Lagrange equations and boundary conditions are

$$\theta''(K_{33}\sin^2\theta + K_{11}\cos^2\theta) + (\theta')^2(K_{33} - K_{11})\sin\theta\cos\theta + \sin\theta\cos\theta(K_{33}(\sin^2\theta - \cos^2\theta) + 2K_{22}\cos^2\theta)(\varphi')^2 + \varepsilon_0\varepsilon_a E^2 \sin\theta\cos\theta = 0 \quad (5a)$$

$$\frac{\mathrm{d}}{\mathrm{d}z}\left(\cos^2\theta\left(K_{33}\sin^2\theta + K_{22}\cos^2\theta\right)\varphi'\right) = 0 \tag{5b}$$

and

$$K_{22}\varphi'(0) + 2(W_1\sin^2\varphi(0) - W_2\cos^2\varphi(0))\sin\varphi(0)\cos\varphi(0) = 0 \tag{6a}$$

$$\theta(0) = \theta(L) = 0;\ \varphi(L) = 0 \tag{6b}$$

respectively. One has to accompany these equations with Maxwell's equations for the electric field:

$$\mathrm{div}\ \mathbf{D} = 0;\ \mathrm{curl}\ \mathbf{E} = 0 \tag{7}$$

where

$$\mathbf{D} = \varepsilon_0\hat{\varepsilon}\mathbf{E} \tag{8}$$

and the elements of the dielectric tensor $\hat{\varepsilon}$ can be expressed in terms of the orthogonal components as

$$\varepsilon_{ij} = \varepsilon_\perp\delta_{ij} + (\varepsilon_\parallel - \varepsilon_\perp)n_in_j \tag{9}$$

in the initial state (when there is no electric field applied). Depending on the ratio between the values of W_1 and W_2, the LC director orientation may be planar ($W_1 \ll W_2$); namely,

$$\theta(z) = 0;\ \varphi(z) = 0 \tag{10}$$

or twisted ($W_1 \gg W_2$)

$$\theta(z) = 0;\quad \varphi(z) = \varphi_0\frac{L-z}{L} \tag{11}$$

We have numerically solved eqn (5)–(9) for the high-birefringence LC used, which has the elastic constants $K_{11} = 10.6 \times 10^{-12}$ N, $K_{22} = 6.36 \times 10^{-12}$ N, $K_{33} = 13.5 \times 10^{-12}$ N (at 20 °C) and the dielectric anisotropy $\varepsilon_a = 10.4$. The effective anchoring energy coefficients for the die-1 nanoantenna array are not known. For some insights on what may happen under the applied voltage, we adopted reasonable values for these coefficients assuming that $W_1 > W_2$. Through numerical modelling we found the following interesting results. At voltages 1–4.5 V and $W_1 = 3 \times 10^{-5}$ J m^{-2}, $W_2 = 1 \times 10^{-5}$ J m^{-2}, only the planar configuration appears in spite of starting to seek a numerical solution from twist as the first guess. However at 5 V, in addition to a planar director configuration a twist configuration also exists when starting to seek a numerical solution from the initial guess of twist. The total free energy for the twist configuration is lower than that for the planar one: -5.1214×10^{-5} J m^{-2} (twist) *vs.* -4.1223×10^{-5} J m^{-2} (planar). Therefore one may expect that, up to 5 V in the dye-1 sample, the LC director is in a planar configuration, becoming twisted at voltages above 5 V, and with a further reorientation to a homeotropic state at a sufficiently high voltage. The detailed modelling of the planar–twist–homeotropic transition will be presented elsewhere.

While the spectra displayed in Fig. 4 are associated with die 1, Fig. 5 demonstrates the weak voltage dependence of plasmonic resonance from a nanoantenna grating. Note that the resonance only occurs in the *x*-direction in the case. The LC molecules structure a 90°-twisted nematic configuration initially. The *x*-polarized incident light then takes a 90° rotation of the polarization state—a phenomenon known as the adiabatic following. When the applied voltage goes beyond 3 V_{rms}, the LC molecules are reoriented vertically and the optical waveguide effect diminishes accordingly such that the polarization of the incident light remains unmodified. It is clear from Fig. 5 that a shutter-like behaviour can be found at 640 nm with a threshold voltage around 3 V_{rms}.

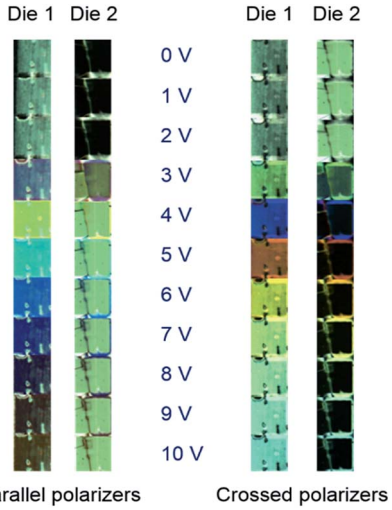

Fig. 6 Polarizing micrographs of the LC cell covering regions of die 1 and die 2.

Fig. 6 shows the images of micrographic textures of the hybrid plasmonic–photonic cell placed between two linear polarizers under the parallel- and crossed-polarizer schemes at various applied voltages. With knowledge of the behaviours of LC on nanoantenna arrays, the color and brightness level of the textures can be easily understood. One can see from Fig. 6 that die 1 exhibits color changes by applied voltages under either polarizer scheme. In contrast, the die-2 plasmonic device exhibits simply a grey-level change between the two voltage regimes separated by the transition voltage of ~3 V_{rms}. It should be reminded that, unlike the case where a regular metallic grating structure is considered,[25] the plasmonic absorption observed in this study relies on multiple periods of the nanostructures. Based on E-beam lithography and suitable LC cell designs, a nanosize-pixeled display or nanoscale optical switch can be further developed.

4. Concluding remarks

In summary, a nanoantenna device comprising a two-dimensional gold nanostructure array (die 1) covered with a high-birefringence LC layer has been studied. By applying voltage on the anisotropic LC layer, we demonstrate that the coupling effect between surface plasmons and photons through the LC can modify the hybrid plasmonic–photonic resonances

in the system. This enables electrical control of the transmission properties rectified by the corresponding plasmonic absorption, yielding a dramatically large wavelength shift of 90 nm in LSPR of the metallic nanoantennas. Our modeling supports the observed results, by assuming that the nanoantenna array leads to two orthogonal easy axes with a finite anchoring energy. The square grooves discussed in Fukuda *et al.*[26] may be considered as a model for our die 1 nanoantenna configuration. Unfortunately we do not know the constant k_s for the LC used in our study, but one could legitimately speculate that the easy axes in the die-1 configuration are along the sides of the squares. We are unaware of any other study else which deals with the electric field-induced director reorientation from the planar to twist and then to the homeotropic configuration with increasing voltage across a LC cell with two easy axes. What one would normally expect is a reorientation from a planar to a homeotropic director configuration; here the "planar–homeotropic" sequence cannot fully explain our experimental observations. Understanding why the "planar–twist–homeotropic" sequence of the LC director profile may occur in our study is important to interpret the observed change in transmittance under increasing applied electric field. As a reference, the spectrum of the LC cell containing an array of strip nanoantennas (die 2) has also been investigated. The transmittance, as can be clearly seen at 640 nm, exhibits a two-level switching effect. An investigation of the LC anchoring for the die-1 and die-2 configurations is beyond the scope of the current paper and will be presented elsewhere. Our current study is about the hybrid plasmonic–photonic resonances in the system and its active control of the spectrum of the metallic nanoantennas. The hybrid structure can be used as a display or a two-level attenuator, making the nanoantenna device promising for photonic applications. A study along the line of optimizing the geometrical distribution of nanoantenna arrays is underway to achieve high contrast for the proposed color filter.

Acknowledgements

This research is financially supported by the Ministry of Science and Technology, Taiwan, under Grant No. MOST 104-2112-M-009-008-MY3 and MOST 104-2221-E-009-130-MY3. VYR and YIC acknowledge the EOARD/STCU grant P521a for financial support.

References

1 P. Bharadwaj, B. Deutsch and L. Novotny, *Adv. Opt. Photonics*, 2009, **1**, 438–483.
2 G. Curto, G. Volpe, T. H. Taminiau, M. P. Kreuzer, R. Quidant and N. F. van Hulst, *Science*, 2010, **329**, 930–933.
3 N. Livneh, A. Strauss, I. Schwarz, I. Rosenberg, A. Zimran, S. Yochelis, G. Chen, U. Banin, Y. Paltiel and R. Rapaport, *Nano Lett.*, 2011, **11**, 1630–1635.
4 T. Coenen, E. J. R. Vesseur, A. Polman and A. F. Koenderink, *Nano Lett.*, 2011, **11**, 3779–3784.
5 M. Hancu, A. G. Curto, M. Castro-López, M. Kuttge and N. F. van Hulst, *Nano Lett.*, 2014, **14**, 166–171.
6 H. Mertens, J. S. Biteen, H. A. Atwater and A. Polman, *Nano Lett.*, 2006, **6**, 2622–2625.
7 T. Ming, L. Zhao, Z. Yang, H. Chen, L. Sun, J. Wang and C. Yan, *Nano Lett.*, 2009, **9**, 3896–3903.
8 P. Anger, P. Bharadwaj and L. Novotny, *Phys. Rev. Lett.*, 2006, **96**, 113002.
9 O. L. Muskens, V. Giannini, J. A. Sánchez-Gil and J. Gomez Rivas, *Nano Lett.*, 2007, **7**, 2871–2875.
10 S. Kühn, U. Håkanson, L. Rogobete and V. Sandoghdar, *Phys. Rev. Lett.*, 2006, **97**, 017402.
11 O. L. Muskens, V. Giannini, J. A. Sánchez-Gil and J. Gomez Rivas, *Nano Lett.*, 2007, **7**, 2871–2875.
12 Y. C. Jun, K. C. Y. Huang and M. L. Brongersma, *Nat. Commun.*, 2011, **2**, 283.
13 V. Shadrivov, P. V. Kapitanova, S. I. Maslovski and Y. S. Kivshar, *Phys. Rev. Lett.*, 2012, **109**, 083902.
14 C. Lumdee, S. Toroghi and P. G. Kik, *ACS Nano*, 2012, **6**, 6301–6307.
15 A. Abass, S. R. K. Rodriguez, T. Ako, T. Aubert, M. Verschuuren, D. Van Thourhout, J. Beeckman, Z. Hens, J. G. Rivas and B. Maes, *Nano Lett.*, 2014, **14**, 5555–5560.
16 P. A. Kossyrev, A. Yin, S. G. Cloutier, D. A. Cardimona, D. Huang, P. M. Alsing and J. M. Xu, *Nano Lett.*, 2005, **5**, 1978–1981.
17 W. Dickson, G. A. Wurtz, P. R. Evans, R. J. Pollard and A. V. Zayats, *Nano Lett.*, 2008, **8**, 281–286.
18 S. Khatua, W.-S. Chang, P. Swanglap, J. Olson and S. Link, *Nano Lett.*, 2011, **11**, 3797–3802.
19 M. Dridi and A. J. Vial, *J. Phys. Chem. C*, 2010, **114**, 9541–9545.
20 K. Chen, E. S. P. Leong, M. Rukavina, T. Nagao, Y.-J. Liu and Y. Zheng, *Nanophotonics*, 2015, **4**, 186–197.
21 W. Dickson, G. A. Wurtz, P. R. Evans, R. J. Pollard and A. V. Zayats, *Nano Lett.*, 2008, **8**, 281–286.
22 H.-W. Su, Y.-H. Lee, M.-J. Lee, Y.-C. Hsu and W. Lee, *J. Biomed. Opt.*, 2014, **19**, 077006.
23 Y.-H. Chen, K.-P. Chen, M.-H. Shih and C.-Y. Chang, *Appl. Phys. Lett.*, 2014, **105**, 031117.
24 J.-I. Fukuda, Y. Makoto and H. Yokoyama, *Phys. Rev. Lett.*, 2007, **98**, 187803.
25 M. Ojima, N. Numata, Y. Ogawa, K. Murata, H. Kubo, A. Fujii and M. Ozaki, *Appl. Phys. Express*, 2009, **2**, 086001.
26 J.-I. Fukuda, J. S. Gwag, M. Yoneya and H. Yokoyama, *Phys. Rev. E: Stat., Nonlinear, Soft Matter Phys.*, 2008, **77**, 011702.

